Available online at www.sciencedirect.com
ScienceDirect
Surface & Coatings Technology 201 (2007) 6117–6121
SURFACE & COATINGS TECHNOLOGY
www.elsevier.com/locate/surfcoat

The influence of the magnetic field configuration on plasma parameters and microstructure of niobium nitride films

S.E. Rodil [a,*], J.J. Olaya [b], S. Muhl [a], B. Bhushan [c], G. Wei [c]

[a] Instituto de investigaciones en materiales, Universidad Nacional Autónoma de México, Circuito Exterior s/n, CU, México D.F. 04510, México
[b] Universidad Nacional de Colombia, Escuela de Ingeniería de Materiales, Facultad de Minas, M3-05, Medellín, Colombia
[c] Nanotribology Laboratory for Information Storage and MEMS/NEMS, Ohio State University, 206 W 18th Avenue, Columbus, OH 43210, USA

Available online 10 October 2006

Abstract

Niobium nitride (NbN) coatings have a variety of interesting properties such as high chemical inertness, excellent mechanical properties, high electrical conductivity, high melting point, and a superconducting transition temperature around 16 K. We have investigated the effects of magnetic field configuration on the plasma characteristic (electron temperature, plasma density, the ion-to-metal flux ratio J_i/J_a and energy parameter E_p) and the microstructure of NbN films grown with a variable magnetron system. The coatings were deposited under identical deposition conditions but with varying the configuration of the magnetic field in the magnetron. The plasma characteristics were determined by planar and cylindrical Langmuir probes for the different magnetic field configurations. The film microstructure and composition were analyzed by X-ray diffraction, scanning electron microscopy and X-ray photoelectron spectroscopy, respectively. The film hardness and Young's Modulus were measured by Nanoindentation.

The variation of the magnetic field with respect to the unbalance state showed that the field changed from a minimum of 3.6 to a maximum of 4.6 mT at the substrate position (5 cm away from target) while in the target center the corresponding values were 49.0 to 98.0 mT, respectively. The lower magnetic field at the target resulted in higher J_i/J_a ratios, plasma densities and potentials. These characteristics resulted in changes in the value of E_p and as this increased the preferred crystalline orientation changed from [200] to [111] and the hardness and Young Modulus increased to 40 GPa and 430 GPa, respectively.
© 2006 Elsevier B.V. All rights reserved.

Keywords: Unbalanced magnetron sputtering; Niobium nitride; Plasma diagnostics; Nanoindentation

1. Introduction

Niobium nitrides are potential candidates for use in variety of applications [1,2]. The high melting point [3], thermal stability [4], chemical inertness [5], and mechanical properties [6–8] such as hardness and toughness make NbN a useful hard coating in extreme conditions.

Several works have shown that the properties of NbN films vary considerably for the different methods of deposition and process parameters used [9–15].

Deposition by DC magnetron sputtering permits a wide variation of deposition parameters which affect the structural and morphological characteristics of the films deposited and consequently, their properties. For example, the ion bombardment during film growth substantially influences the electronic and mechanical properties. The main parameters that describe the ion bombardment are the ion energy, E_i, and the ion/atom flux ratio J_i/J_a. Both parameters show an influence on the structure and properties of films deposited by ion-assisted methods [16–19]. Unbalanced magnetron sputtering is an effective system to control the ion bombardment since the magnetic field configuration directs some of the ions from the plasma towards the substrate, and this can be used to modify the properties of the films [20]. The aim of the present work was to better understand the role of the magnetic field configuration on both the plasma and film properties.

2. Experimental setup and procedure

The NbN films were deposited using unbalanced (Teer Coatings Ltd.) and balanced (Vacuum Inc.) magnetron

* Corresponding author. Tel.: +52 5556224734; fax: +52 5556161251.
E-mail address: ser42@iim.unam.mx (S.E. Rodil).

0257-8972/$ - see front matter © 2006 Elsevier B.V. All rights reserved.
doi:10.1016/j.surfcoat.2006.08.120

sputtering cathodes. The magnetic field of the unbalanced system is controlled by the relative position of the magnets connected to a threaded bar, so that the unbalance is directly proportional to the number of turns (N_v) of the bar. All films were deposited using a 4-in. diameter 99.95% purity Nb target, in an N_2/Ar atmosphere (both of ultra high purity). The substrate was positioned 5 cm from the target and the substrate temperature was kept at 380 °C. The chamber base pressure was $<7\times10^{-4}$ Pa and the working pressure was 0.9 Pa using a total gas flow of 16 sccm, with the Ar/N_2 flow-rate ratio fixed at 7. The DC discharge power for all samples was 200 W and the coating thickness was approximately 1.8 μm. In the case of the unbalanced system, films were deposited at values of N_v (0 to 5) and for comparison samples were prepared using the balanced magnetron sputtering cathode (BM) using the same deposition conditions. Substrates of 4 cm^2 pieces of silicon were used for the structural and compositional analysis, 3 cm diameter discs of high-speed steel (AISI M2) were used for the hardness tests.

The magnetic field was measured using a hall probe portable gaussmeter, Walker Scientific MG-4D. The field perpendicular and parallel to the target was measured as function of the radial distance from the front of the target, r, the separation from the target surface, z, and for the unbalanced cathode as a function of N_v.

The plasma parameters were determined from the current-voltage data from a cylindrical probe using the software developed by Camps et al. [21] and the ion current densities, J_i, were measured using a 0.125 mm^2 planar probe at a DC bias of −100 V. All measurements were made at the substrate position at 5 cm from the centre of the target.

The crystalline structure was analyzed using a Siemens D5000 X-ray diffractometer using Cu-K_α radiation and a Ni filter. The measurements were made in steps of 0.02 degree for 14 s in the 2θ range from 30 to 120. The grain size for the different crystalline directions were calculated from the full width half maximum of the appropriate peaks using the Scherrer equation. The texture factors for the samples were obtained from the ratio of the integral of counts in the peak of interest to that of the sum of all of the observed peaks. The surface chemical compositions of the films were characterized by X-ray photoelectron spectroscopy (XPS) using a Thermo-scientific Multilab and MgK_α radiation. A stylus perfilometer DEKTAK IIA was used to measure film thickness. The hardness was determined with an ultra-micro hardness tester MXTBO-UL with 0.025 kg of load. The nanohardness and the elastic modulus were measured using a Nanoindenter II R (MTS Systems Corp.). This instrument monitors and records the dynamic load and displacement of a three sided pyramidal diamond indenter (Berkovich) during indentation with a force resolution of about 75 nN and displacement resolution of about 0.1 nm. Multiple loadings and unloading steps were performed to examine the reversibility of the deformation, ensuring that the unloading data used for analysis are mostly elastic. The corrosion resistance of the NbN coatings was evaluated by potentiodynamic polarization scans in 0.5 M H_2SO_4 containing 0.05 M KSCN.

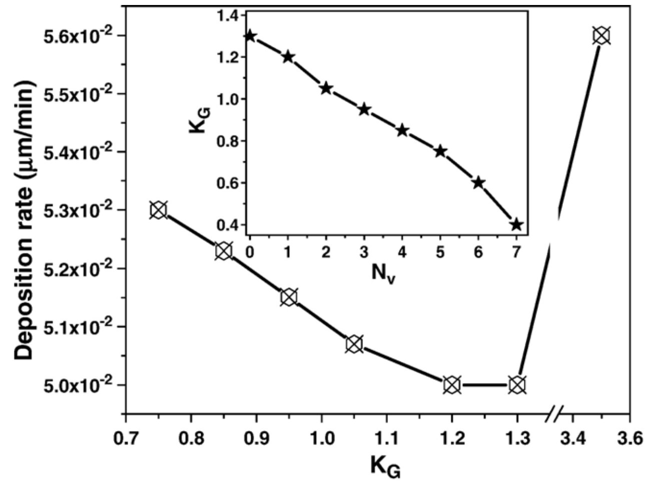

Fig. 2. The deposition rate is plotted as a function of the unbalance coefficient, K_G. The insert shows the variation of K_G as a function of the number of turns, N_v.

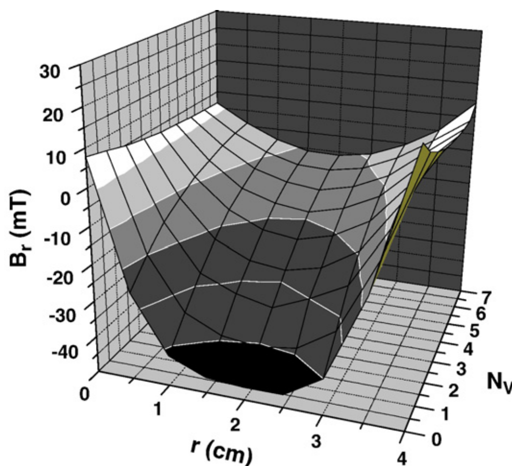

Fig. 1. The radial variation, r, of the magnetic field parallel to the target surface, B_r, directly in front of the target, $z=0$, as a function of the number of turns, N_v.

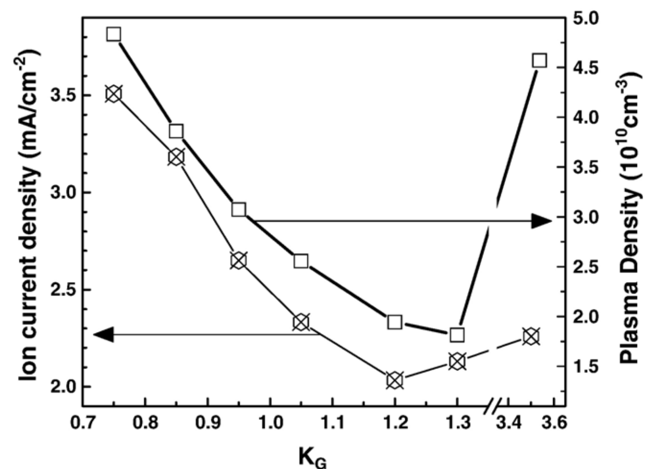

Fig. 3. The ion current incident on the substrate and the plasma density as a function of the unbalance coefficient, K_G.

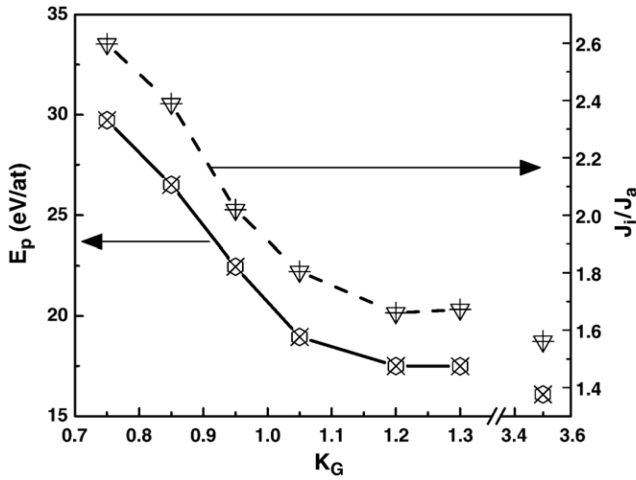

Fig. 4. The energy-per-deposited atom, E_p, and the ion to atom flux ratio, J_i/J_a, as a function of the unbalance coefficient, K_G.

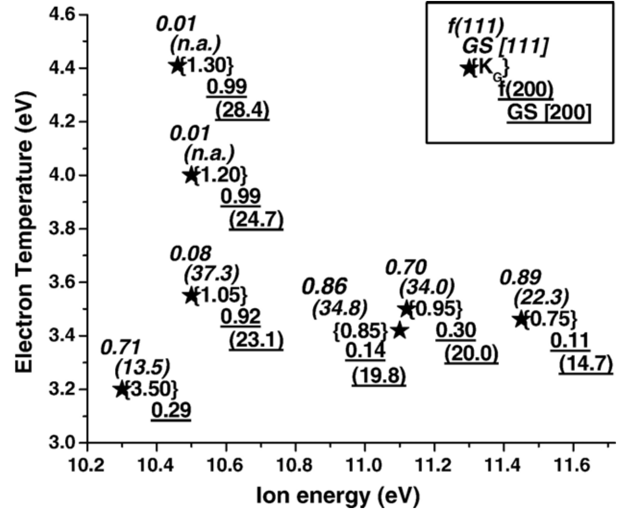

Fig. 6. The electron temperature is plotted against the ion energy, E_i. The crystallographic texture factor and grain size for the [111] and [200] directions, and the unbalance coefficient is provided for each data point, see key in the figure, n.a. indicates data not available, GS[hkl] and f(hkl) are the grain size and crystallographic texture factors for the (111) and (200) orientations, K_G is the unbalance coefficient.

The value of I_{crit} was estimated from the maximum anodic dissolution current before passivation [22].

3. Results

The Fig. 1 shows the radial component of the magnetic field in front of the target in function of the number of turns of the internal magnetic assembly of the magnetron and the radial distance from the centre of the target. The maximum value, 48.5 mT, is at a radial distance of 2 cm. On the other hand, at the substrate position, 5 cm from the target, the magnetic field was approximately uniform and perpendicular to the substrate surface, i.e. B_z, with a value of 4.7 mT 1.5 cm either side of the central position, $r=0$. The degree of unbalance of magnetrons can be quantified through the K_G coefficient defined as; $K_G = \frac{d_{B_{z=0}}}{2R_t}$, where R_t is the average radius of the erosion zone (for our cathode this is 2 cm), and $d_{B_{z=0}}$ is the distance from the target to where B_z=0 [23]. Values greater than 3 represent a balanced magnetron. The insert in Fig. 2 shows how K_G varies with N_v. The Fig. 2 shows that the deposition rate decreases slightly with the degree of unbalance of the magnetron and is somewhat greater for the balanced magnetron which estimated value is K_G=3.5. The Fig. 3 presents the ion current density incident on the substrate and plasma density versus the unbalance coefficient. Both of the plasma parameters tend to decrease with increasing K_G but the plasma density is notably high for the balanced cathode. The ratio of the ion flux and deposited atom flux, J_i/J_a, and the energy per deposited atom, E_p, values [24] were calculated as a function of K_G from

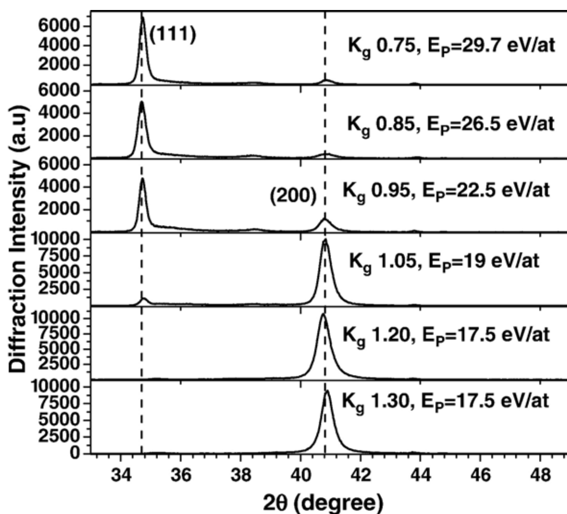

Fig. 5. XRD spectra obtained from the samples under different conditions of ion bombardment.

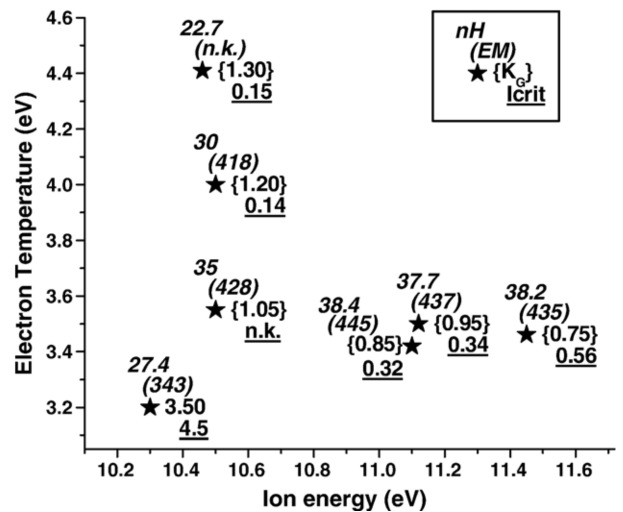

Fig. 7. The same axes are used as in Fig. 6 to present a mapping of the nanohardness, elastic modulus and critical corrosion current, together with the unbalance coefficient for each data point, see key in the figure, I_{crit}, nH, EM are the critical corrosion current density, nanohardness and elastic modulus respectively, K_G is the unbalance coefficient (n.k. indicates data not measured).

the deposition rate, the Langmuir probe and ion current density measurements, assuming a volumetric film density of the bulk value of NbN (8.43 g/cm^3). These results are shown in Fig. 4 together with the values for the balanced magnetron.

The chemical analysis of the deposits showed that the Nb/N ratio was equal to 1 ± 0.1 for all values of K_G.

The Fig. 5 shows the X-ray diffraction spectra obtained for the films deposited at different values of K_G, with the appropriate values of K_G and E_P for the magnetic field configurations. In the full spectra, not shown, only those diffraction peaks related to the [111] and [200] orientations of the FCC phase of δ-NbN (JCPDS No. 38-1155), together with a small peak at $2\theta \approx 118°$ which corresponds to the [422] cubic δ-NbN phase, were observed. For E_p values greater than 20 eV/atom, $K_G < 1$, there are a number of small peaks, ∼ 62°, which might be associated with δ′-NbN hexagonal phase (JCPDS No. 14-0547).

The Fig. 6 shows the relationship between the crystallographic structure and the ion energy, E_i, and the electron temperature, T_e. The graph shows a mapping of the values of the texture factors and grain sizes for the [111] and [200] directions, together with the value of K_G, in terms of E_i and T_e.

The Fig. 7 shows a similar mapping of the hardness, elastic modulus and critical current from the corrosion testing in terms of E_i and T_e.

4. Discussion

It is important to note that in this design of a variable unbalanced magnetron as the degree of unbalance is increased, decrease of K_G or increase of N_v, the intensity of the radial magnetic field strongly decreases. This might be considered to mean that for the strongest magnetic field, $K_G = 1.3$ the least unbalanced configuration, the plasma density should be greatest resulting in the highest sputtering rate and therefore the highest deposition rate. The results given in Figs. 4 and 3 show that exactly the opposite was observed. The explanation of this is probably related to the idea of the unbalanced magnetron. The Fig. 5 shows that up to 2.6 times more ions than atoms arrive at the substrate and, from Fig. 4, the ion flux increases as the degree of unbalance increases; this being exactly the objective of the unbalanced magnetron. In fact the deposition rate was found to increase linearly with the ion current flux indicating that a constant proportion of the ion flux corresponds to film precursor ions. Obviously mass spectrometry measurements are needed to confirm this idea.

The crystallographic texture appears, in Fig. 6, to vary according to the value of E_p, however the data for the balanced magnetron does not agree with this trend. However, if the plasma density is also considered, a good agreement for all of the data is obtained. Various authors have suggested explanations of the variation of the crystallographic orientation in terms of the overall free energy of the film, W_{hkl}, with this being the sum of the surface energy, S_{hkl}, and the strain energy, U_{hkl} [25,26], where the surface energy is related to the existence of unsaturated bonds in the surface atoms and can be expressed as

$$S_{hkl} = (N_{hkl} \times L_s)/(Z \times N_a)$$

where N_{hkl} is the number of unsaturated bonds per atom in the (hkl) plane, L_s is the sublimation energy, Z is the coordination number and N_a is Avogadro's number [26]. The strain energy for the two-dimensional case with equal principal stress can be expressed as

$$U_{hkl} = \varepsilon_{hkl}^2 \times E_{hkl}(1 - \nu)$$

where ν is the Poisson's ratio, ε_{hkl} is the strain and E_{hkl} the Young's modulus in the (hkl) lattice plane of the film [26].

Unfortunately data is not available for NbN but on the basis of the similarity of the crystal and mechanical properties of TiN, TiC and NbN we assume that the same relative values of S_{hkl}, ε_{hkl}, E_{hkl} and ν can be used. As the thickness of films increases the orientation is expected to change from the [100] to the [111] direction as the strain energy dominates [26]. Ion bombardment increases the strain energy component; therefore under conditions of high bombardment the orientation change occurs at lower thickness [27].

Other models have been presented to describe the effect of low energy (≤20 eV) ion bombardment during film growth [28,29]. The proposed idea was that this energy is sufficient to cause collisional dissociation of the N_2^+ ions providing a source of atomic nitrogen. The nitrogen readily chemisorbs on the (100) planes but not on the N-terminated (111) planes. This reduces the mean free path of the metal cation on the (100) plane due to capture and promotes the formation of $MetN_i$ ($i = 1$–4) islands. This can be considered as causing an additional decrease in the (100) surface energy relative to that of the (111) plane. Consequently, the presence of the nitrogen atoms reduces the flux of cations from the (100) to the (111) planes, resulting in the orientation of the growth in the [100] family of directions.

Now the relative concentration of nitrogen precursors generated in the plasma under conditions of identical gas pressure, gas mixture and applied power might be estimated from the electron temperature and the plasma density since to a first approximation the precursors are produced by electron energy transfer processes. In our case the measured plasma density cannot be used because we know that near the substrate this decreases as the radial magnetic field increases (increasing K_G) due to greater plasma confinement and indeed it appears that the plasma density near the target actually increases. From Fig. 6 we can see that for $T_e < 3.5$ eV the films have a preferred [111] orientation and with increasing ion energy the texture factor increases. At the lowest E_i and T_e the film orientation is a mix of [111] and [200]. However, as the T_e increases the films become more and more [200] and the grain size increases, in agreement with the models described above.

The other film properties can also be mapped using the T_e versus E_i approach. Fig. 7 shows that only films made using an $E_i > 11$ eV have a hardness of greater than 35 GPa and an elastic modulus greater than 430 GPa. For coatings deposited on metal substrates only the metal part at the bottom of the pinholes or defects are subject to active dissolution in corrosion testing. Therefore, I_{crit} is proportional to the exposed area of the substrate at the bottom of the pinholes and is therefore a measure of the porosity of the films [30]. From Fig. 7 it can be seen that the

value of I_{crit} is strongly influenced by the plasma T_e and appears to be almost independent of E_i although more work is required to clarify this aspect.

5. Conclusions

Under the experimental conditions studied, the crystallographic orientation of the NbN films was controlled by a combination of the degree of ion bombardment and the flux of reactive nitrogen species at the growing film surface. Films could be produced under conditions of high ion bombardment with a hardness in excess of 38 GPa.

Acknowledgements

We wish to acknowledge the financial support of the DGAPA through the projects IN100701, IN100203 and IX108004, and also to thank Leticia Baños and Lazaro Huerta for their help with the XRD and XPS analysis of the films.

References

[1] A. Rando, C. Peacock, A.V. Foden, J. Dordrecht, Lumley, C. Pereire, J. Appl. Phys. 73 (1993) 5096.
[2] G.N. Goltsman, A.D. Semenov, Y.P. Gousev, M.A. Zorin, I.G. Gogidze, E.M. Gershenzon, P.T. Lang, W.J. Knott, K.F. Renk, Supercond. Sci. Technol. 4 (1991) 453.
[3] D.R. Lide (Ed.), CRC Handbook of Chemistry and Physics, 82nd ed., CRC Press LLC, 2001–2002, p. 4.
[4] L. Hultman, Vacuum 57 (2000) 1.
[5] M. Fenker, M. Balzer, R.V. Buchi, H.A. Jehn, H. Kappl, J.-J. Lee, Surf. Coat. Technol. 163–164 (2003) 169.
[6] K.S. Havey, J.S. Zabinski, S.D. Walck, Thin Solid Films 303 (1997) 238.
[7] F. Lévy, P. Hones, P.E. Schmid, R. Sanjine´s, M. Diserens, C. Wiemer, Surf. Coat. Technol. 120– 121 (1999) 284.
[8] A. Bendavid, P.J. Martin, T.J. Kinder, E.W. Preston, Surf. Coat. Technol. 163– 164 (2003) 347.
[9] M.J. Deen, D. Landheer, J.D. Wade, G.I. Sproule, M.D. Denhoff, J. Vac. Sci. Technol., A 6 (1988) 2299.
[10] R.L. Boxman, V.N. Zhitomirsky, I. Grimberg, L. Rapoport, S. Goldsmith, B.Z. Weiss, Surf. Coat. Technol. 125 (2000) 257.
[11] K. Baba, R. Hatada, K. Udoh, K. Yasuda, Nucl. Instrum. Methods, B 127/128 (1997) 841.
[12] A. Bendavid, P.J. Martin, T.J. Kinder, E.W. Preston, Surf. Coat. Technol. 163–164 (2003) 347.
[13] P.J. Kelly, R.D. Arnell, Vacuum 56 (2000) 159.
[14] K.S. Havey, J.S. Zabinski, S.D. Walck, Thin Solid Films 303 (1997) 238.
[15] M. Fenker, M. Balzer, R.V. Buchi, H.A. Jehn, H. Kappl, J.-J. Lee, Surf. Coat. Technol. 163–164 (2003) 169.
[16] P.J. Kelly, R.D. Arnell, Surf. Coat. Technol. 97 (1997) 595.
[17] I.V. Svadkovski, A.P. Dostanko, D.A. Golosov, S.M. Zavatskiy, D.A. Kotov, Third International Conference on Plasma Physics and Plasma Technology, Minsk, Belarus, vol. 2, 2000, p. 716.
[18] J. Musil, Vacuum 50 (1998) 363.
[19] S. Kadlec, J. Musil, Vacuum 47 (3) (1996) 307.
[20] P.H. Mayrhofer, C. Tischler, C. Mittterer, Surf. Coat. Technol. 142–144 (2001) 178.
[21] E. Camps, R. Ordiza, G. Anguiano, Rev. Mex. Fis. 38 (1992) 825 (Spanish).
[22] D.A. Jones, Principles and prevention of corrosion, Prentice Hall, Upper Saddle River, NJ, 1996.
[23] I.V. Svadlovski, D.A. Golosov, S.M. Zavatskiy, Vacuum 68 (2003) 283.
[24] J. Musil, S. Kadlec, Vacumm 40 (1990) 435.
[25] J. Pelleg, L.Z. Zevin, S. Lungo, Thin Solid Films 197 (1991) 117.
[26] J.P. Zhao, X. Wang, Z.Y. Chen, S.Q. Yang, T.S. Shi, X.H. Liu, J. Phys., D Appl. Phys. 30 (1997) 5.
[27] U.C. Oh, Jung Ho Je, J. Appl. Phys. 74 (1993) 1692.
[28] I. Petrov, P.B. Barna, L. Hltman, J.E. Greene, J. Vac. Sci. Technol., A 21 (2003) S117.
[29] D. Gali, S. Kodambaka, M.A. Wall, I. Petrov, J.E. Greene, J. Appl. Phys. 93 (2003) 9086.
[30] H. Uchida, S. Inoue, K. Koterazawa, Mater. Sci. Eng., A Struct. Mater.: Prop. Microstruct. Process. 649 (1997) 234.